

Efficient sampling in materials simulation - exploring the parameter space of grain boundaries

Holger Dette, Josua Goesmann, Christian Greiff^a, Rebecca Janisch^{b,*}

^a*Department of Mathematics, Institute of Statistics, Ruhr-Universität Bochum, 44780 Bochum, Germany*

^b*Interdisciplinary Centre for Advanced Materials Simulation (ICAMS), Ruhr-Universität Bochum, 44780 Bochum, Germany*

Abstract

In the framework of materials design there is the demand for extensive databases of specific materials properties. In this work we suggest an improved strategy for creating future databases, especially for extrinsic properties that depend on several material parameters. As an example we choose the energy of grain boundaries as a function of their geometric degrees of freedom. The construction of existing databases of grain boundary energies in face-centred and body centred cubic metals relied on the a-priori knowledge of the location of important cusps and maxima in the five-dimensional energy landscape, and on an as-densely-as-possible sampling strategy. We introduce two methods to improve the current state of the art. The location and number of the energy minima along which the hierarchical sampling takes place is predicted from existing data points without any a-priori knowledge, using a predictor function. Furthermore we show that it is more efficient to use a sequential sampling in a “design of experiment” scheme, rather than sampling all observations homogeneously in one batch. This sequential design exhibits a smaller error than the simultaneous one, and thus can provide the same accuracy with fewer data points. The new strategy should be particularly beneficial in the exploration of grain boundary energies in new alloys and/or non-cubic structures.

Keywords: sequential sampling; design of experiment; grain boundary energy; atomistic simulations; high-throughput methods

1. Introduction

Increasing computational power contributes to the creation and extension of huge materials databases containing a variety of material properties. Such data collections can form the the basis for material design and discovery, and thus promise great savings in development time and costs. The materials project [1] or the NOMAD repository [2] which together feature roughly $3.5 \cdot 10^6$ entries (state of July 28th, 2016) are impressive examples of such property collections. They can be used to search for correlations in property maps, or as input for material models.

High-throughput numerical simulations play a key role in determining materials properties, because they allow a systematic variation of individual parameters, such as composition, and the coverage of a broad range of these parameters. Nevertheless, the majority of properties that are available today are so-called intrinsic properties like stability, stiffness, or band gaps. Extrinsic properties, that depend on additional structural

*rebecca.janisch@rub.de

parameters, like interface energies or mobilities, are less frequently available. As a matter of fact, because they depend on several of variables at the same time, such properties form multidimensional databases of their own for one particular material. For such cases we want to promote with the paper at hand an efficient sampling of the variable space that is based on design of experiment principles. As a suitable example we pick grain boundary energies, which depend on five geometric degrees of freedom.

The evolution of a microstructure of a metallic or multiphase material during solidification or deformation depends to a large extend on the energy of the interfaces in the microstructure. So do the resulting macroscopic properties, the deformability, thermal stability, and strength. Substantial scientific effort is put into describing the interactions of individual defects that form the microstructure within and across different material length scales to model their influence on the macroscopic properties. Again, numerical simulations are a valuable tool in this respect, because they allow the isolation of specific effects on different length or time scales, as well as the abovementioned systematic variation of parameters that enter any material model.

In this paper we focus on grain boundaries, i.e. homophase interfaces, which separate two regions of undistorted crystal of the same crystal structure and chemistry that are misoriented with respect to each other. The space of macroscopic geometric parameters that define a grain boundary structure is five-dimensional - three degrees of freedom for the misorientation of the grains, two for the interface inclination. It is not per se clear which sampling strategy is the best for this five dimensional space. An intuitive approach might be to sample the parameter space homogeneously as finely as possible, so that afterwards an interpolation between the points is possible without knowing the underlying function that connects them. Alternatively, one can rely on a so-called structure model, which helps to identify the slowly and quickly varying regions in the energy function. Ideally, it already provides a closed form expression for the energy as a function of the structural parameters. This latter approach has been recently used by Bulatov et al. [3] to find a universal function for the crystallography class of face-centered cubic (fcc) metals. It reduces the amount of required data points, but uses a-priori knowledge of the topography of the multi-dimensional space of macroscopic parameters defining the grain boundary geometry. In particular it requires the specification of the number and the location of the cusps and maxima in the energy landscape. The 3D rotational subspaces that represent energy minima can indeed be predicted based on crystal symmetry. To a large extend, especially for fcc metals, the positions of the cusps in the one-dimensional subspaces of energy as a function of misorientation for twist and tilt grain boundaries can be predicted fairly well based on a random grain-boundary model [4], or a lattice-matching approach [5]. However, they depend on the details of the atomistic structure and hence on the nature of the interatomic bonding, which makes a prediction more difficult already for bcc metals [5], and especially for systems with directional bonds such as diamond or silicon no straight forward relationship exists [6].

In this paper we show that the method proposed by Bulatov et al. [3] can be significantly improved in at least two directions. First we develop an estimate, which does not require any knowledge of the number and the location of cusps and maxima of the energy function, but determines these parameters from the data. Secondly, we address the problem of efficient sampling in such experiments. In contrast to previous work, which considers curve fits from all available data (within a subspace) we propose a sequential approach. A first part of the sample is used to obtain a prediction for the energy function. Subsequent sampling is performed sequentially, such that the new experiment is conducted at sampling points, where the uncertainty of the prediction for the derivative of the energy function is maximal. Additionally, the prediction is continuously updated using the new information of the previous experiments. Doing so we can

minimize the number of points which are necessary to give a reliable description of the parameter space, especially cusps and maxima in the energy landscape. Thus, the important parameters of the energy function do not have to be known a priori, and still the computational effort remains manageable.

The remaining part of this paper is organized as follows. In Section 2 we give a brief description of the geometry and structure of the grain boundary and describe the existing data bases of grain boundary energies. We also describe the structural model introduced in [3] which will be further developed in this paper. Section 3 introduces the new statistical methodology, and the advantages of the sequential sampling approach are illustrated in Section 4.

2. Grain boundary structure and energy

The geometry and structure of grain boundaries are determined by the five macroscopic and three microscopic degrees of freedom (DOF), i.e. by

- the misorientation of the two grains, e.g. defined by rotation axis $\hat{\rho}$ and angle x , or a rotation matrix \mathbf{A} , which rotates grain 1 into grain 2. This rotation determines three macroscopic DOF.
- the inclination of the grain boundary plane, defined by its normal vector $\hat{\mathbf{n}}$, that determines the remaining two macroscopic DOF.
- a translation \mathbf{t} of the grains parallel and perpendicular to the interface plane, which fixes the three microscopic DOF.

Traditionally, grain boundaries for which the plane normal vector $\hat{\mathbf{n}}$ is perpendicular to the misorientation axis $\hat{\rho}$ are called tilt grain boundaries, those with $\hat{\mathbf{n}}$ parallel to $\hat{\rho}$ twist grain boundaries.

Several other representations of the grain boundary geometry are possible, e.g. a representation by two rotation matrices that describe the orientation of each grain with respect to a reference frame, in which one axis is perpendicular to the interface. It depends on the application which representation is the most convenient one. For instance, a representation by two rotation matrices is useful to construct grain boundary structures as input for atomistic simulations, as done e.g. in [7]. However, to evaluate afterwards the energies of grain boundaries as a function of their degrees of freedom, as done e.g. by Wolf [8] for face centred cubic metals, a representation in terms of rotation axis and angle is more descriptive.

Some grain misorientations lead to a periodic superstructure across the grain boundary, a so-called “coincidence site lattice” (CSL). CSL-based grain boundaries represent low-energy structures that are especially important when trying to capture the material properties. Hence, besides being characterised by their misorientation they are usually described by an additional parameter Σ , which is the ratio of the CSL unit cell volume to that of the original crystal lattice unit cell. In other words it is a measure for the periodicity of the CSL lattice.

In principle the energies of all possible grain boundary structures in a microstructure could be determined from atomistic simulations. The only limiting factors are the computational demand and the availability of a reliable description of the interatomic interactions. Indeed, databases are being created and expanded that include several thousand structures.

Up to date there exist two major collections of grain boundary energies which were obtained from atomistic simulations, the database of Kim et al. [9] for body-centred cubic (bcc) iron, and the one of

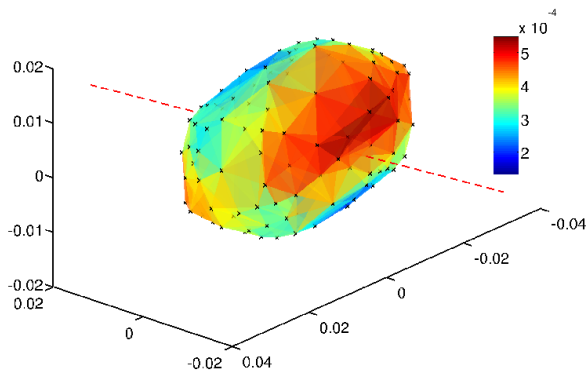


Figure 1: Energy as a function of plane inclination for a $\Sigma 9$ misorientation (data from [9]).

Olmsted and co-workers [7] for face-centred cubic (fcc) aluminium and nickel, and a more recent version also for bcc iron. The structure of the databases reflects two different approaches: Kim et al. sample the 5D parameter space as densely as possible in a homogeneous fashion, i.e. for arbitrary misorientations, to provide sufficient data for a numerical interpolation scheme. Details are given in Section 2.1.

In the approach chosen in [7] the emphasis is put on the CSL-based grain boundaries by sampling the subspace of special misorientations around high-symmetry axes in the cubic lattice. Thus, in the resulting database the minimum energy regions are represented well, but to interpolate safely in the “non-special regions” a model for the energy as a function of the geometric degrees of freedom is needed. This has been provided by [3], as described below in Section 2.2

2.1. Homogeneous sampling and numerical interpolation

In the work of Kim et al. the misorientation between two bcc grains is represented by the three Euler angles between a reference coordinate system (grain 1) and a sphere inside (grain 2). The misorientation range is then sampled by dividing each Euler angle into nine equal intervals of 10 degrees ($0 \leq \phi_1 \leq 90^\circ, 0 \leq \Phi \leq 90^\circ, 0 \leq \phi_2 \leq 90^\circ$), leading to 729 misorientations. For a smooth energy function of the misorientation, this might have been a sufficiently dense sampling. However, this homogeneous scheme misses the majority of the special misorientations, which lead to CSL boundaries and to pronounced cusps in the energy function. This is a striking example of the fact that even a strictly systematic parametric study can miss the most important features of a target function, and it motivates again our improved scheme which is able to identify such points. Kim et al. were aware of the missed features in the topology of the parameter space and thus additional 26 CSL boundaries with $\Sigma \leq 33$ were constructed separately. For each misorientation, special or non-special different inclinations of the grain boundary plane were selected, representing equally spaced points on the sphere, in total 91 inclinations. Figure 1 shows the anisotropy of the energy as a function of plane inclination for a $\Sigma 9$ misorientation extracted from the database of Kim et al. [9].

This anisotropy is an important factor for the evolution of the microstructure e.g. during grain growth. With their dense sampling [9] et al. were able to provide enough data points for interpolation within a phase-field model in the simulation of grain growth in polycrystalline iron of [10]. This demonstrates on the one hand the usefulness of such databases, but on the other hand also their limitations. The next step towards a more realistic material system would be to include a second chemical (alloying) element in

the grain boundary structure. In principle, grain boundary energies in a multi-component system could be obtained by a similar procedure as used for the database for pure Fe grain boundaries. However, a good description of the five-dimensional space of geometric degrees of freedom already required including 66.339 structures, each obtained as result of a multi-step optimisation procedure. Every alloying element would add another compositional degree of freedom to the five geometric ones, and thus increase the number of structures by orders of magnitude.

2.2. Fitting in subspaces and hierarchical interpolation

An alternative strategy was chosen by Bulatov et al. [3], who fitted the parameters of a five-dimensional energy function to the database of Olmsted. Starting point for the construction of this function is the dislocation model for grain boundaries [11]. It describes a grain boundary as a two-dimensional array of lattice dislocations. The energy of this array is the sum of the energies of the individual dislocations, which can be calculated e.g. according to elasticity theory (with the core energy being a free parameter). Strictly speaking this picture breaks down if the density of the dislocations in the grain boundary becomes so large that the dislocation cores start to overlap, i.e. for misorientation angles around 10° . Wolf showed [12], however, that the expression of Read and Shockley [11] can be extended piecewise to the complete range of misorientation angles between 0° and 180° , as shown schematically in Figure 2. The resulting model, though fully empirical, can be justified by the existence of grain boundary dislocations with Burgers vectors that can assume (continuous and) much smaller values than the one of lattice dislocations and thus exist in array much more dense.

Wolf defined such functions for the one-dimensional subspaces of symmetrical tilt and twist grain boundaries, i.e. $E(x)$ for fixed rotation axes, of the type

$$E(x) = \sin(\pi/2 x)(E_c - E_s \log(\sin(\pi/2 x))) \quad (1)$$

in which x varies between 0 and 1. E_s is the strain energy of the dislocation, which can be approximated by $E_s = Gb/2\pi$, with the material parameters shear modulus G and Burgers vector b [8]. E_c is the dislocation core energy, which was used as adjustable parameter to fit the model to grain boundary energies determined via atomistic simulations.

In [3] equation (1) is re-phrased by splitting off a dimensionless part

$$f_{\text{RSW}}(x) = \sin(\pi/2 x)(1 - a \log(\sin(\pi/2 x))) \quad (2)$$

for each segment of the one dimensional functions, which is then multiplied with the energy of the maximum in the respective segment and (scaled and) shifted to the corresponding interval. For a precise definition see formula (3) in the following section. With respect to the formulation of Wolf, a could be regarded as the ratio of strain to core energy, but in fact it is a fit parameter.

Reference energies for several hundred grain boundaries in different fcc metals are available from the work of Olmsted et al. [7], who carried out atomistic simulations using EAM type potentials. As mentioned the sampling of the 5D space is not homogeneous in this case, but is restricted to misorientations around high-symmetry axes of cubic crystals that lead to coincidence site lattices. This way 388 grain boundaries with 72 different misorientations around the $\langle 111 \rangle$, $\langle 110 \rangle$, and $\langle 100 \rangle$ axes of the fcc lattice were constructed. As pointed out in [3], this approach is reasonable if one assumes that the topography of the GB energy

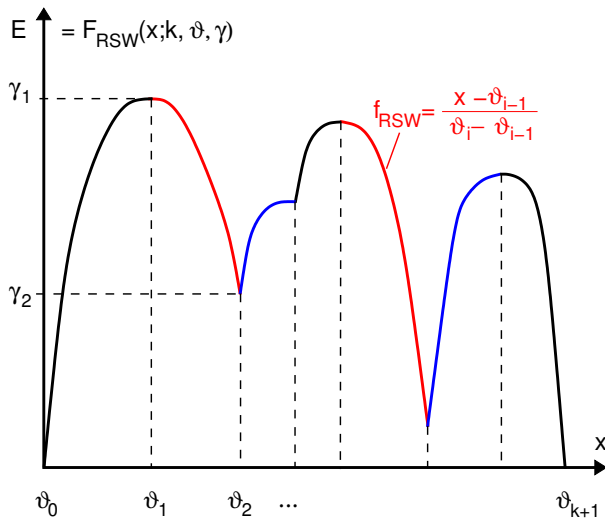


Figure 2: Schematic of the 1D subspace of energy as a function of misorientation (of twist or symmetrical tilt grain boundaries). The function is expressed piecewise between two change points ϑ_{i-1} and ϑ_i by the Read-Shockley model (1) (rescaled to the interval $[\vartheta_{i-1}, \vartheta_i]$). In this work we explore ways to determine the number of necessary segments f_{RSW} efficiently.

function is defined by cusps or “grofs” of order k , special subsets of the 5-dimensional space of macroscopic DOF, for which the energy is minimal with respect to variations locally orthogonal to the set. In other words, the energy is smooth along the valley of the $(N - k)$ dimensional subset, but forms a cusp in the complementary k -subspace. The connectivity of grofs is defined by the crystal symmetries.

Accordingly, Bulatov et al. [3] started by fitting the one dimensional scaffolding sets of symmetrical tilt and twist boundaries with misorientation axes $\langle 100 \rangle, \langle 111 \rangle, \langle 110 \rangle$. In the next step the 2D subset including asymmetric tilt grain boundaries was obtained by interpolating between these six 1D sets, and the 3D scaffolding sets of mixed grain boundaries (neither pure twist nor tilt) in turn by interpolating between the 2D subsets. In a last step the interpolation between the 3D scaffolding sets in 5D space was done by approximating the energy of an arbitrary grain boundary as a weighted average over the energies of all best-matching boundaries found within the three 3D scaffolding subsets. This is equal to assuming a rather flat 2D subspace of energy vs. plane inclination. This assumption of a slowly varying function for the energy as a function of plane inclination is a rather strong one, as can be seen from the results of [9], see e.g. Figure 1. Apart from this, a comparison of four different fcc metals shows that the fitting function is rather universal, since 27 of the 42 dimensionless parameters turned out to be more or less the same for all investigated materials.

To summarize, the importance of the CSL boundaries motivates the “special” sampling approach [7] followed by a hierarchical interpolation scheme [3], starting with the subspaces of grain boundaries with misorientations around high symmetry axes, rather than using a homogeneous sampling scheme over the whole 5D space. However, since the 2D subspace of plane inclinations is by no means flat (especially not in a multi-component system), a sampling of this subspace, which is more or less neglected in the data of [7], has to be included, as done in [9].

3. Improved statistical inference of the grain boundary energy function

As mentioned, an important feature in the description of the topography of the grain boundary energy subspaces are the energy-cusps. Olmsted et al. [7] and Bulatov et al. [3] investigate the grain boundary energy function for fcc models with a-priori knowledge of the number and location of the cusps. The Read-Shockley-Wolf (RSW) function proposed in [12] is used to model the energy values of grain boundaries in these subspaces [3]. In this work we introduce an alternative procedure, which improves the current state of the art in at least two directions.

- First - in contrast to [3] - we determine the location and number of the cusps and maxima for the RSW model directly from the available data. Recall from Section 2 that the energy function consists of piecewise models of the form (2) rescaled on different intervals as displayed in Figure 2. We propose to determine the number and the location (more precisely the left and right end-point) of these intervals from the available data. This gives a fit of RSW model without using any a-priori information.
- Secondly, we propose an efficient way of locating profitable measurement spots. This is achieved by a sequential sampling scheme. A first part of the sample is used for a prediction of the energy function. Subsequent sampling is then performed sequentially, such that the new experiment is conducted at sampling points, where the uncertainty of the prediction for the derivative of the energy function is maximal. Additionally, the prediction is updated after each experiment. Thus we address the problem of the high computational costs in these numerical experiments, and minimize the number of points which are necessary to give a reliable description of the topography of these subspaces.

3.1. Estimating a RSW-Function

In this section we describe a general approach to estimate all parameters in a piecewise RSW model. As introduced in section 2.2, the RSW-segment function is given by

$$f_{\text{RSW}}(x) = \sin(\pi/2x)(1 - a \log(\sin(\pi/2x))) ,$$

where x varies between 0 and 1. Now let k denote the (unknown) number and $0 = \vartheta_0 < \vartheta_1 < \dots < \vartheta_k < \vartheta_{k+1} = \vartheta_{\text{max}}$ the (unknown) boundary points of the intervals in which different RSW segments are used. ϑ_{max} depends on the rotational symmetry of the misorientation axis in question. For instance, the $\langle 110 \rangle$ directions in a cubic lattice have two-fold rotational symmetry, thus $\vartheta_{\text{max}} = 180^\circ$, while the $\langle 100 \rangle$ axes have four-fold rotational symmetry and $\vartheta_{\text{max}} = 90^\circ$. The boundary points may correspond to cusps, local maxima, or shoulders of the energy function, as schematically shown in Figure 2. Throughout this paper these points will be called *change points*. Moreover, we denote by $\gamma_0 = 0$ the energy at point $\vartheta_0 = 0$. We define a piecewise RSW function F_{RSW} of the order k with energy levels $\gamma_1, \dots, \gamma_k$ by

$$F_{\text{RSW}}(x; \vartheta, \gamma, k) = \sum_{i=1}^{k+1} I_{[\vartheta_{i-1}, \vartheta_i]}(x) \left[I_{[-\infty, 0]}(\gamma_i - \gamma_{i-1}) \cdot \left(\gamma_i + (\gamma_{i-1} - \gamma_i) \cdot f_{\text{RSW}}\left(\frac{\vartheta_i - x}{\vartheta_i - \vartheta_{i-1}}\right) \right) \right. \\ \left. + I_{[0, \infty]}(\gamma_i - \gamma_{i-1}) \cdot \left(\gamma_{i-1} + (\gamma_i - \gamma_{i-1}) \cdot f_{\text{RSW}}\left(\frac{x - \vartheta_{i-1}}{\vartheta_i - \vartheta_{i-1}}\right) \right) \right] \quad (3)$$

where

$$I_{[a, b]}(\kappa) = \begin{cases} 1 & \text{if } \kappa \in [a, b] \\ 0 & \text{otherwise.} \end{cases}$$

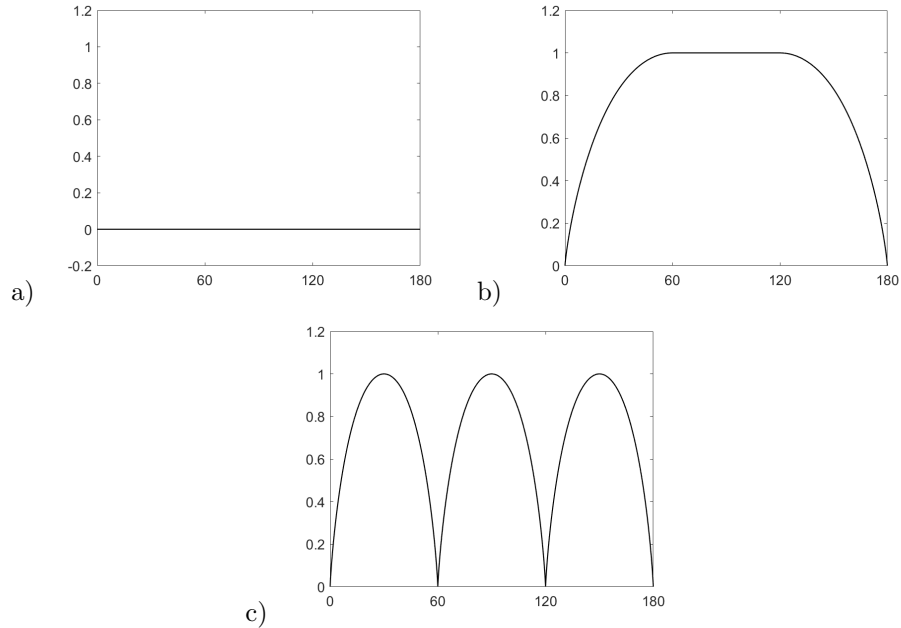


Figure 3: Examples of RSW energy functions $F_{\text{RSW}}(x)$ for different parameters k , ϑ and γ . A choice of such functions is also used as starting points in the minimization of (4). a) $k = 0$ and $\gamma = 0$, b) $k = 2$, $\vartheta_1 = 60^\circ$, $\vartheta_2 = 120^\circ$ and $\gamma_1 = \gamma_2 = 1$ c) $k = 5$, $\vartheta_1 = 30^\circ$, $\vartheta_2 = 60^\circ$, $\vartheta_3 = 90^\circ$, $\vartheta_4 = 120^\circ$, $\vartheta_5 = 150^\circ$, $\gamma_1 = \gamma_3 = \gamma_5 = 1$ and $\gamma_2 = \gamma_4 = \gamma_6 = 0$

$I_{[a,b]}(x)$ denotes the indicator function that assigns the different RSW-segment functions f_{RSW} to their intervals $[\vartheta_{i-1}, \vartheta_i]$ ($\kappa = x$), respectively determines the sign of the segment ($\kappa = \gamma_i - \gamma_{i-1}$). Note that in equation (3) ϑ and γ are short notations for the complete sets of angles and energies, $\vartheta = (\vartheta_1, \dots, \vartheta_k)$, and $\gamma = (\gamma_1, \dots, \gamma_{k+1})$. Each specification (k, ϑ, γ) corresponds to a different energy function. For example, if $k = 0$ and $\gamma_0 = 0$, the energy as a function of misorientation is constant, as shown in Figure 3a). The combination $k = 2$, $\vartheta_1 = 60^\circ$, $\vartheta_2 = 120^\circ$ and $\gamma_1 = \gamma_2 = 1$ gives the function shown in figure 3b), and $k = 5$, $\vartheta_1 = 30^\circ$, $\vartheta_2 = 60^\circ$, $\vartheta_3 = 90^\circ$, $\vartheta_4 = 120^\circ$, $\vartheta_5 = 150^\circ$, $\gamma_1 = \gamma_3 = \gamma_5 = 1$ and $\gamma_2 = \gamma_4 = \gamma_6 = 0$ would yield the function displayed in Figure 3c). In the following sections we discuss the problem of fitting a piecewise RSW function to data $\{(x_i, E_i) \mid i = 1, \dots, n\}$, where the pair (x_i, E_i) denotes the i th observation of a grain boundary with misorientation angle x_i and corresponding simulated energy E_i . This means that we have to determine the number of change points k , locations $\vartheta = (\vartheta_1, \dots, \vartheta_k)$, and heights $\gamma = (\gamma_1, \dots, \gamma_{k+1})$ of the (unknown) RSW-function F_{RSW} from the data.

3.1.1. Estimating a RSW-Function with fixed number of change points

In [3] it is assumed that the number k and the location of (some of) the change points $\vartheta_1, \dots, \vartheta_k$ are known, and the values $\gamma_1, \dots, \gamma_k$ are determined from the grain boundary energies in the database of [7]. In this section we take the first step to a more flexible approach by assuming that only the number of change points is known (for example from symmetry properties of the crystal) and the other parameters have to be determined from the available data. The problem of additionally determining the number k from the data will then be addressed in the next section.

The estimation of the parameters $\vartheta_1, \dots, \vartheta_k$ and $\gamma_1, \dots, \gamma_{k+1}$ can then be done by a constrained non-linear

least squares approach minimizing the sum of squared errors

$$\text{SSQ}(\vartheta, \gamma) = \frac{1}{n} \sum_{j=1}^n [E_j - F_{\text{RSW}}(x_j, \vartheta, \gamma, k)]^2 \quad (4)$$

with respect to (ϑ, γ) under the constraints $\vartheta_{i-1} \leq \vartheta_i$ ($i = 1, \dots, k+1$). The minimization is realized by the non-linear optimization algorithm SQP (see e.g. [13]), which is implemented e.g. in the optimization routine "fmincon()" of ©MATLAB. Note that the corresponding optimization problem is not convex. Consequently, the quality of these algorithms depends sensitively on the set of starting points. To ensure reliable results every minimization was performed with the three different starting sets. Possible examples of such functions are displayed in Figure 3) and we used the best of the three obtained minimizers. These values are denoted by $\hat{\vartheta}$ and $\hat{\gamma}$. In the statistical literature $\hat{\vartheta}$ and $\hat{\gamma}$ are usually called (*constrained*) *least squares estimates* as the sum of squares is minimized under the constraints $\vartheta_{i-1} \leq \vartheta_i$ ($i = 1, \dots, k+1$).

If one evaluates the RSW function F_{RSW} for a given angle x and the estimates $\hat{\vartheta}$, $\hat{\gamma}$ one obtains a prediction $\text{pred}(x) := F_{\text{RSW}}(x, \hat{\vartheta}, \hat{\gamma}, k)$ of the unknown RSW function $F_{\text{RSW}}(x, \vartheta, \gamma, k)$ at the point x . As $\hat{\vartheta}$, $\hat{\gamma}$ contain a statistical estimation error it is of particular interest to specify the uncertainty of this prediction. For this purpose we require some mathematical assumptions and assume that the statistical model is given by

$$E_i = F_{\text{RSW}}(x_i, \vartheta, \gamma, k) + \varepsilon_i, \quad i = 1, \dots, n \quad (5)$$

where $\varepsilon_1, \dots, \varepsilon_n$ are independent identically distributed random variables with mean 0 and the variance σ^2 . In (5) the variable ε_i denotes a random error which is introduced to model deviations from the functional relation $y = F_{\text{RSW}}(x, \vartheta, \gamma, k)$, which ideally describes the relation between energy y and angle x through the RSW function. It then follows from standard results of mathematical statistics (see for example [14]) that the variance of the prediction $\text{pred}(x)$, for the energy at point x is approximately given by

$$\text{Var}(\text{pred}(x)) \approx \hat{V}^2(x) := \text{SSQ}(\hat{\vartheta}, \hat{\gamma}) \cdot m(x, \hat{\vartheta}, \hat{\gamma}) \left(\sum (m(x_i, \hat{\vartheta}, \hat{\gamma})^T m(x_i, \hat{\vartheta}, \hat{\gamma})) \right)^{-1} m(x, \hat{\vartheta}, \hat{\gamma})^T \quad (6)$$

where

$$m(x, \hat{\vartheta}, \hat{\gamma}) = \left(\frac{\partial}{\partial \vartheta} F_{\text{RSW}}(x, \vartheta, \gamma, k) \Big|_{\vartheta=\hat{\vartheta}, \gamma=\hat{\gamma}}, \frac{\partial}{\partial \gamma} F_{\text{RSW}}(x, \vartheta, \gamma, k) \Big|_{\vartheta=\hat{\vartheta}, \gamma=\hat{\gamma}} \right)$$

denotes the gradient of the piecewise RSW function evaluated at the estimates $\hat{\vartheta}$ and $\hat{\gamma}$. This means that the standard error of the prediction is approximately given by $\hat{V}(x)$. Obviously we are interested in predictions with a *small* standard error for all angles of interest.

3.1.2. Determining the number \hat{k} of change points

The estimation method discussed in Section 3.1.1 requires the specification of the number of change points k , which is often not available in simulations of grain boundary energies. In this section we use an *information criterion* from mathematical statistics to determine the unknown order k of the function in equation (3) from the available data, i.e. we determine the number of segments f_{RSW} from which F_{RSW} . Roughly speaking, such a criterion is used to balance the complexity and the quality of a parametric fit of the energy function. For example, in an extreme case, one would just interpolate the data using a model with a large number of parameters. Obviously, such a model would be useless, because the number of parameters coincides with the number of data points. On the other hand a model with too few parameters might not

give a reasonable fit to the observed data. For detailed discussion of statistical model selection the reader is referred to [15].

Consider a piecewise RSW function $F_{\text{RSW}}(x, \vartheta, \gamma, k)$ of a fixed order k and let $(\hat{\vartheta}^{(k)}, \hat{\gamma}^{(k)})$ denote the (constrained) least squares estimates determined by the procedure described in Section 3.1.1. The *Bayesian Information Criterion* (BIC) is given by

$$\text{BIC}(k) := n \log(\text{SSQ}(\hat{\vartheta}^{(k)}, \hat{\gamma}^{(k)})) + k \log(n) , \quad (7)$$

where SSQ is the sum of squares defined in equation (4) and n is the number of data points. The order of the RSW function is now estimated by the value \hat{k} for which $\text{BIC}(k)$ is minimal, that is

$$\hat{k} = \text{argmin}_k \text{BIC}(k) .$$

If the minimum is attained at two (or more) values, say \hat{k}_1, \hat{k}_2 we choose the smaller value as estimate of the order. The estimates of the parameters are the values $(\hat{\vartheta}^{(\hat{k})}, \hat{\gamma}^{(\hat{k})})$ corresponding to the optimal value \hat{k} . Note that by increasing the order k we increase the number of parameters in the RSW function and the sum of squares in equation (4) decreases. Therefore, the first term $n \log(\text{SSQ}(\hat{\vartheta}^{(k)}, \hat{\gamma}^{(k)}))$ in equation (7) becomes smaller, if the number of parameters in the model is increased. However this decrease is penalized by the second term $k \log(n)$ which increases with k . Thus, by minimizing the Bayesian Information criterion one tries to obtain a reasonably good fit (that is a small value for the sum of squared deviations between the observed data and the predicted values) with a reasonably small number of parameters. General mathematical arguments as given in [15] show that the BIC criterion estimates the unknown order of the model correctly if the sample size is reasonable large and the “true” model is in fact a piecewise RSW function.

3.2. Sequential design of experiments

In this section we describe the estimation procedure which simultaneously estimates the model (including the number and location of the change points) and additionally determines the location of the new data points in an efficient way. We suggest this procedure to replace any sampling strategy in which the number and spacing of data points to obtain (e.g. from atomistic simulations) is fixed prior to the screening run. Note that in the following the term “experiment” is used in the sense of “numerical simulation”. The steps are the following:

- (1) (Initialization) Start with an initial sample of size n_0 , say $\{(x_i, E_i) \mid i = 1, \dots, n_0\}$, of experiments taken (for example from an homogeneous design) on the given interval, which is $[0, 45]$, $[0, 60]$, $[0, 90]$ or $[0, 180]$.
- (2) (n_s further sequential experiments) For $j = n_0, \dots, n = n_0 + n_s$ do
 - (2.1) (Estimation of parameters) Determine a fit $F_{\text{RSW}}(x, \hat{\vartheta}_j, \hat{\gamma}_j, \hat{k}_j)$ of the RSW function from the data points $\{(x_i, E_i) \mid i = 1, \dots, j\}$. For this purpose we determine the estimates $\hat{k}_j, \hat{\vartheta}_j, \hat{\gamma}_j$ using the least squares method and the BIC criterion described in Section 3.1.1 and 3.1.2.

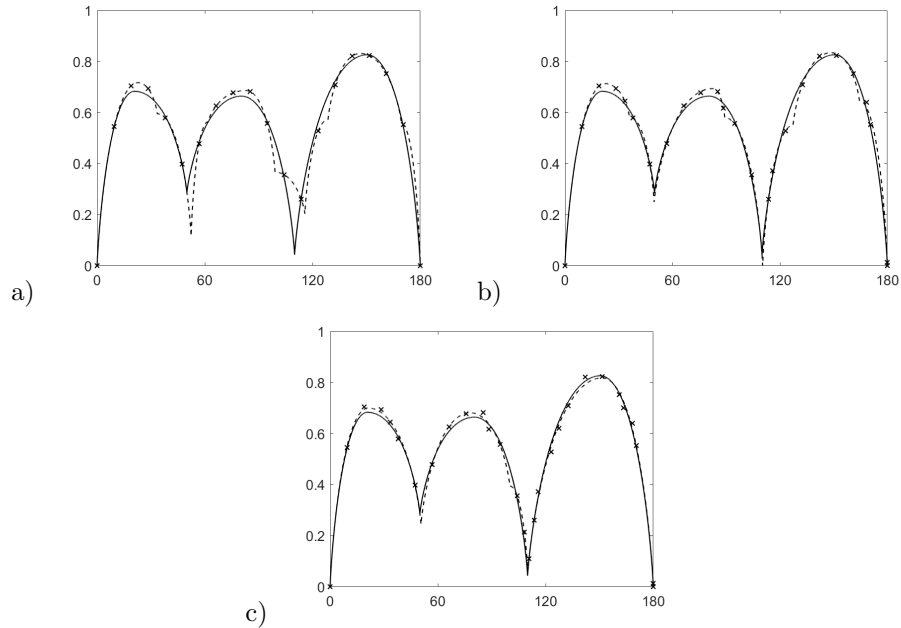


Figure 4: Estimates (dashed curves) of function F_2 (solid curves) for sample sizes 20, 25 and 30. After 20 initial points (homogeneously sampled), all further points have been obtained by the sequential procedure described in Section 3.2.

(2.2) (Find the next point) Calculate a prediction $\text{pred}_j(x)$ for any point x of interest, where the uncertainty of the prediction is specified by the function $\hat{V}(x)$ defined in (6). The next point x_{j+1} is then determined as the maximizer of the function $\hat{V}(x)$. In other words we run the next simulation under an experimental condition x_{j+1} , where we expect the largest uncertainty. Interestingly, in the simulated examples the maximum variance is not necessarily obtained between the points with a maximum variation of the misorientation angle. The outcome of this experiment is denoted by E_{j+1} .

(2.3) (Increase the sample size) Put $j \leftarrow j + 1$

3.3. Example

In this section we give a brief illustration of the estimation and sequential sampling procedure proposed in the previous paragraphs. Suppose, that the true model is given by the function F_2 , which is shown in Figure 6. In order to estimate this function we run 20 experiments homogeneously sampled over the interval $[0, 180]$, which corresponds to the initial step in Section 3.2. The estimate of the function F_2 based on this starting set is displayed by a dashed curve in Figure 4a) (the solid curve represents the “true” function F_2). The next points are then sampled sequentially as described in the previous section. In Figure 4b) we display the estimate (dashed curve) on the basis of 5 additionally sampled points (this means that here the total sample size is 25). We observe, that the quality of the estimate has already improved. Performing the sequential procedure five further times, we can estimate the function on the basis of 30 observations and the result is shown in Figure 4c). The quality of the estimate has further improved and the function F_2 is nearly reconstructed.

4. Empirical results

In this section we present a simulation study investigating the differences between sequential and homogeneous sampling for the one-dimensional space of misorientation angles. Note that instead of carrying out an atomistic simulation to obtain the grain boundary energy for a given misorientation angle, we have simply used the model (5) to calculate it. Thus, the simulated data points follow piecewise a RSW-curve (subject to a random error), but we pretend this is not known and estimate it instead. To mimic the deviations which usually occur, between the results of real atomistic simulations and an idealized model of grain boundary energies, we have added a normal distributed measurement error.

The experimental conditions x_1, \dots, x_n , in this case the angles for which we require the grain boundary energies, were obtained in two ways. First the misorientation space was sampled homogeneously with n homogeneous points x_1, \dots, x_n . This method will be denoted by (M1) in the following discussion. Secondly, we applied the sequential procedure proposed in Section 3.2 to determine the n experimental conditions, where we used homogeneous designs of different sizes as initial sample. This method will be denoted by (M2).

We have simulated data according to model (5) with a normal distributed measurement error with variance of 0.02. Six different RSW functions are investigated which are taken from [3] and are displayed in Figure 6. The RSW functions F_1 , F_2 and F_3 belong to the sets symmetric of tilt grain boundaries with fixed misorientation axis $\langle 100 \rangle$, $\langle 110 \rangle$ and $\langle 111 \rangle$, respectively. The other triple F_4 , F_5 and F_6 belongs to the sets of twist grain boundaries with fixed misorientation axis $\langle 100 \rangle$, $\langle 110 \rangle$ and $\langle 111 \rangle$, respectively. For simplicity, the shape parameter a given in [3] was set to $a = 0.5$, which only affected functions F_4 and F_6 . In Table 1 and 2 we display the simulated error

$$\max_x |F_{\text{RSW}}(x, \hat{\vartheta}, \hat{\gamma}, \hat{k}) - F_{\text{RSW}}(x, \vartheta, \gamma, k)|$$

between the estimated and “true” piecewise RSW function $F_{\text{RSW}}(x, \vartheta, \gamma, k)$ for the function F_1 , F_2 , F_3 and F_4 , F_5 , F_6 , respectively. All results are based on 1000 simulation runs at each step j . For comparison of the different sampling strategies, we limited the number of observations (grain boundary energies) to fit the RSW function by $n = 50$. The first column of each table shows how many points were chosen homogeneously in the initial step, while the second columns gives the number of points chosen sequentially. This means that

n_0	n_s	F_1	F_2	F_3
50	0	0.059938	0.04323	0.0097287
40	10	0.06776410	0.05616720	0.0079849
30	20	0.07095250	0.03322720	0.00789995
20	30	0.07381860	0.04987090	0.00778615
10	40	0.07965220	0.08002340	0.00787698

Table 1: Simulated estimation error for different designs and the RSW functions F_1 , F_2 , F_3 defined in [3] and shown in Figure 6. The total number of measurement points (misorientation angles), n , is always 50, of which n_0 were chosen in a homogeneous fashion in the initial step, and n_s sequentially at positions of maximum uncertainty. Thus, the first row in the table corresponds to a completely homogeneous sampling scheme, the last row to a mostly sequential one. The numbers in bold face mark the smallest estimation error for the different designs. For more details see text.

n_0	n_s	F_4	F_5	F_6
50	0	0.003103	0.019071	0.010073
40	10	0.0030438	0.0164675	0.00809395
30	20	0.0031124	0.0167076	0.0080853
20	30	0.0032427	0.0174876	0.008056
10	40	0.002992	0.0176678	0.00767696

Table 2: Simulated estimation error for different designs and the RSW functions F_4 , F_5 , F_6 defined in [3] and shown in Figure 6. The total number of measurement points (misorientation angles) is n is always 50, of which n_0 were chosen in a homogeneous fashion in the initial step, and n_s sequentially at positions of maximum uncertainty. Thus, the first row corresponds to a completely homogeneous sampling scheme, the last row to a mostly sequential one. The numbers in bold face mark the smallest estimation error for the different designs. For more details see text.

the first row of each table represents the results of sampling method (M1), where no points have been chosen sequentially and misorientation angles are chosen by completely by an homogeneous design in the initial step. Similarly, e.g. the third row with the values 30 and 20 is the first and second columns correspond to the sequential method (M2) with an initial design of size 30 and a sequential design of size 20 in the second step. In this case the simulated estimation error for the function F_2 is given by 0.03322720. The numbers printed in boldface show the best estimation error for the different designs. For example, for the function F_1 the non-sequential design is the best, while the sequential design with 30 observations in the initial step yields a a 18% larger error. Similarly for the function F_3 the sequential design with 10 observations in the initial step is the best and the non-sequential design has a 25% larger error.

We finally compare the sequential design with sample size 30 in the initial step (third line in both tables) with the non-sequential design (first line in the tables). For the function F_1 the latter design shows a better performance. On the other hand, in all other cases the sequential design yields a smaller estimation error, where the improvement varies between 15% and 25%. Thus the sequential approach seems to be an interesting alternative to homogeneous sampling.

A particular important question in applications is how many observations are needed to obtain a fit of the RSW function with an estimation error smaller than a given level. To investigate this issue we consider the performance of a non-sequential and a sequential design with 60% of the observations in the first step for different sample sizes. In Figure 5 we display exemplarily the estimation error in the estimation of the function F_2 and F_5 , where the sample size varies between 20 and 100. For example, if the sample size is 40, the sequential design takes 24 observations in the first step and 16 observations are taken sequentially as described in Section 3.2. 1000 simulation runs have been used to calculate this error. For the RSW function F_2 we observe a better performance of the new sequential sampling scheme, whenever the sample size is larger than 40 and this design yields always smaller estimation error for the function F_5 .

The results in Figure 5 can also be interpreted in the following way. Assume that one is interested in the estimation of the function F_5 with an error not larger than 0.020. If one uses a non-sequential design, 60 observations are required to achieve this precision, while the same precision can be obtained with only 40 measurements sampled according to the sequential design. These results demonstrate the benefits of the sequential sampling approach proposed in this paper.

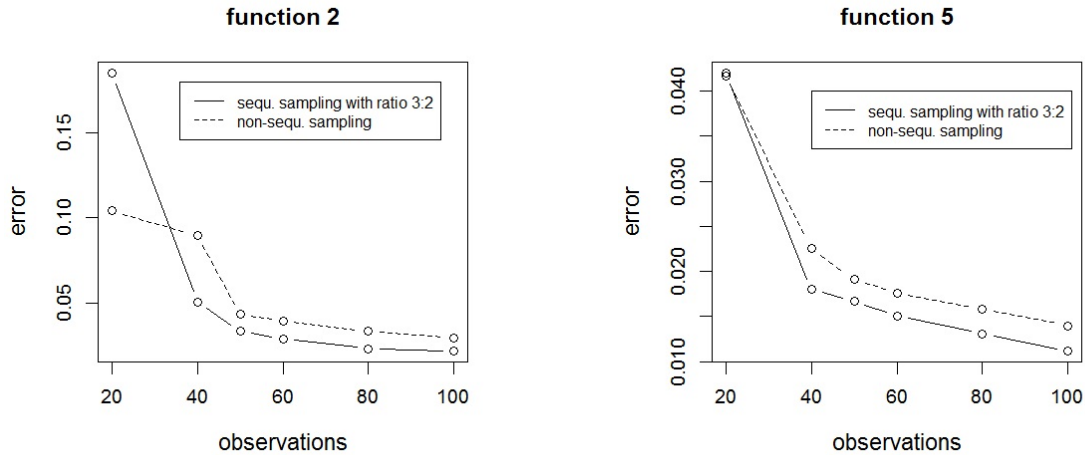


Figure 5: Estimation error of fits from a sequential (solid line) and non-sequential design (dashed line) for various sample sizes for RSW functions F_1 and F_5 .

5. Summary and Conclusion

In the framework of materials design there exists an increasing demand for databases of specific materials properties. In this work we have reviewed two major collections of grain boundary energies that were created from atomistic simulation data and suggest an improved strategy for creating future databases.

The database of Kim et al. [9] is based on a homogeneous sampling of the misorientation as well as the plane-inclination subspace, extended by the energies of special grain boundaries that were missed in the homogeneous scheme. In contrast, the database of Olmsted and co-workers [7] is restricted to several subsets of special misorientations. In combination with a physics based interpolation function as suggested by Bulatov [3] the latter seems more efficient, but in the current state is lacking sufficient data in the plane-inclination subspace.

In any case both schemes rely on the a-priori knowledge of the location of important cusps and maxima in the five-dimensional energy landscape of grain boundaries. We suggest two ways to improve the current state of the art. Firstly, the location and number of the energy minima along which the hierarchical sampling takes place, can be predicted from existing data points without any a-priori knowledge, using a predictor function. Second, instead of a sampling a fixed number of equally spaced data points in a given subspace, we show that it is more efficient to use a sequential sampling in a “design of experiment” scheme. This sequential design exhibits a smaller estimation error than the simultaneous one, and thus can provide the same accuracy with fewer data points. This new strategy should be particularly beneficial in the exploration of extrinsic material properties, if the “property landscape” has a unknown topography, for example grain boundary energies in new alloys and/or non-cubic structures.

Acknowledgements. This work has been supported in part by the Collaborative Research Center “Statistical modeling of nonlinear dynamic processes” (SFB 823, Project C1, C2) of the German Research Foundation (DFG).

- [1] A. Jain, S. P. Ong, G. Hautier, W. Chen, W. D. Richards, S. Dacek, S. Cholia, D. Gunter, D. Skinner, G. Ceder, K. a. Persson, The Materials Project: A materials genome approach to accelerating materials innovation, *APL Materials* 1 (1) (2013) 011002.
- [2] NOMAD, <http://nomad-repository.eu/cms/>, version of July 28, 2016, ????
- [3] V. Bulatov, B. Reed, M. Kumar, Grain boundary energy function for fcc metals, *Acta Mater.* 65 (2014) 161–175.
- [4] D. Wolf, A broken bond model for grain boundaries in face-centered cubic metals, *J. Appl. Phys.* 68 (1990) 3220–3236.
- [5] B. Runnels, I. J. Beyerlein, S. Conti, M. Ortiz, An analytical model of interfacial energy based on a lattice-matching interatomic energy, *J. Mech. Phys. Solids* 89 (2016) 174–193.
- [6] O. Shenderova, D. Brenner, Atomistic simulations of structures and mechanical properties of polycrystalline diamond: Symmetrical $\langle 001 \rangle$ tilt grain boundaries, *Phys. Rev. B* 60 (1999) 7043–7052.
- [7] D. L. Olmsted, S. M. Foiles, E. A. Holm, Survey of computed grain boundary properties in face-centered cubic metals: I. Grain boundary energy, *Acta Mater.* 57 (2009) 3694–3703.
- [8] D. Wolf, Correlation between structure, energy, and ideal cleavage fracture for symmetrical grain boundaries in fcc metals, *J. Mater. Res.* 5 (1990) 1708 – 1730.
- [9] H.-K. Kim, W.-S. Ko, H.-J. Lee, S. G. Kim, B.-J. Lee, An identification scheme of grain boundaries and construction of a grain boundary energy database, *Scripta Mater.* 64 (2011) 1152–1155.
- [10] H.-K. Kim, S. G. Kim, W. Dong, I. Steinbach, B.-J. Lee, Phase-field modeling for 3D grain growth based on a grain boundary energy database, *Modelling Simul. Mater. Sci. Eng.* 22 (2014) 034004–19.
- [11] W. Read, W. Shockley, Dislocation Models of Crystal Grain Boundaries, *Physical Review* 78 (1950) 275 – 289.
- [12] D. Wolf, A Read-Schockley model for high-angle grain-boundaries., *Scripta Metall* 23 (1989) 1713–1718.
- [13] J.-F. Bonnans, J. C. Gilbert, C. Lemarechal, C. A. S. et.al, *Numerical Optimization: Theoretical and Practical Aspects (Universitext)*, Springer, 2nd edn., 2006.
- [14] P. J. Bickel, K. A. Doksum, *Mathematical Statistics, Basic Ideas and Selected Topics, Vol. 1,2, (2nd Edition)*, Pearson Prentice Hall, New Jersey, 2006.
- [15] G. Claeskens, N. L. Hjort, *Model Selection and Model Averaging*, Cambridge University Press, Cambridge, 2008.

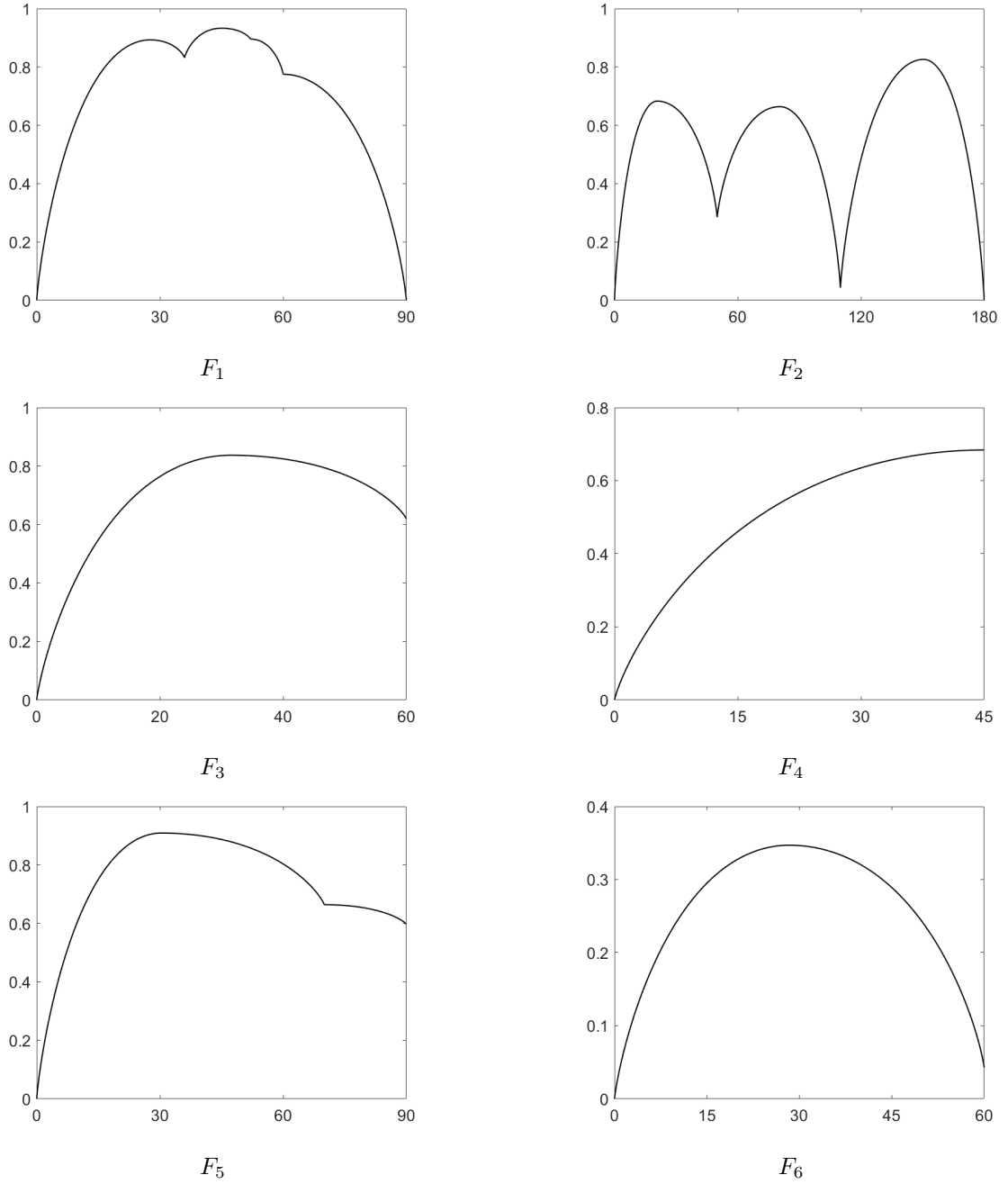


Figure 6: Six RSW energy functions considered in [3]. The RSW functions F_1 , F_2 and F_3 belong to the sets symmetric of tilt grain boundaries with fixed misorientation axis $\langle 100 \rangle$, $\langle 110 \rangle$ and $\langle 111 \rangle$, respectively. The other triple F_4 , F_5 and F_6 belongs to the sets of twist grain boundaries with fixed misorientation axis $\langle 100 \rangle$, $\langle 110 \rangle$ and $\langle 111 \rangle$, respectively. Note that, the shape parameter a given in [3] was set to $a = 0.5$, which only affected functions F_4 and F_6 .